Maxwellian Material-Based Absorbing Boundary Conditions for Lossy Media in 3-D

David C. Wittwer, *Member, IEEE,* and Richard W. Ziolkowski, *Fellow, IEEE*

***Abstract*—A two time-derivative Lorentz material (2TDLM), which has been shown previously to be the correct Maxwellian medium choice to match an absorbing layer to a lossy region, is extended here to a complete absorbing boundary condition (ABC) for three-dimensional (3-D) finite-difference time-domain (FDTD) simulators. The implementation of the lossy 2TDLM (L2TDLM) ABC is presented. It is shown that in contrast to the one-dimensional (1-D) and two-dimensional (2-D) versions, the full 3-D ABC requires a three time-derivative Lorentz material in the edge and corner regions to achieve a rigorous matching of the resulting Maxwellian absorbing layer to the lossy medium. The 3-D ABC implementation thus requires the introduction of an auxiliary field to handle the edge and corner regions to achieve a state–space form of the update equations in the ABC layers. Fully 3-D examples including pulsed dipole radiation and pulsed Gaussian beam propagation in lossless and lossy materials as well as pulse propagation along a microstrip over lossless and lossy materials are included to illustrate the effectiveness of the L2TDLM ABC.**

***Index Terms*—Lossy media, perfectly matched layers.**

I. Introduction

CONSIDERABLE effort has been expended in recent years both in the computational electromagnetics (CEM) [1]–[22] and applied mathematics communities [23], [24] toward the construction of highly efficient absorbing boundary conditions (ABC's) for reflectionless grid truncation of numerical simulators for Maxwell equations. Ideally, the perfect ABC would absorb electromagnetic energy incident from any angle, with any polarization and at all frequencies. Reflectionless termination of simulation regions associated with, for instance, finite-difference time-domain (FDTD) and finite-element (FEM) methods require such ABC's. Generally, the perfectly matched layer (PML) or the related uniaxial ABC's have only been applied to terminate lossless regions of the simulation space [9]–[24].

Unfortunately, many practical simulation problems involving, for instance, microstrip transmission lines, microstrip patch antennas, and microwave/millimeter wave integrated circuits (MIC/MMIC), deal with lossy substrates. Accurate simulations of these problems necessitate termination of the simulation region with an ABC matched to these lossy dielectrics. Several papers have appeared recently [1]–[8] which have established the need for such lossy media ABC's and have proposed partial or complete solutions. Berenger's PML ABC cannot be applied directly in this case; it was developed for the termination of a lossless dielectric region. For instance, Rappaport and Winton [3] have demonstrated the need for lossy media ABC's with their modeling of ground probing radar signals in lossy dispersive soil. Gedney in [4] and [8] developed an uniaxial PML (UPML) ABC that avoids the field splitting associated with the Berenger PML ABC. Results for the UPML ABC applied in two dimensions to a current filament radiating in air over a lossy half-space were given. Lau *et al.* [5], Fang and Wu [6], and Liu [7] introduced variations of the Berenger PML ABC to deal with evanescent wave and lossy media problems. These approaches use the stretched coordinate ideas and normal field splitting associated with the Berenger PML ABC. An example of a line source in a two-dimensional (2-D) homogeneous lossy medium was given in [5]; a line source radiating in a 2-D layered lossy medium was given in [6]. A three-dimensional (3-D) lossless microstrip line problem was discussed in [6]. A qualitative graphical presentation of comparisons with analytical solutions for a dipole source in a homogeneous 3-D homogeneous lossy medium and scattering from a conductive sphere in a 3-D homogeneous lossy medium were given in [7]. Additional issues associated with ABC's for various media situations have been reviewed by Gedney in [8, ch. 5].

The focus of this paper is the development of a complete 3-D Maxwellian material-based ABC for the truncation of FDTD simulation regions dealing with general lossy dielectrics in three dimensions. This is accomplished with a generalized formulation of the two time-derivative Lorentz material (2TDLM) approach that has been shown previously to be the correct Maxwellian medium choice to match an absorbing layer to a lossy dielectric region [1]. It is shown here that in contrast to the 2TDLM absorbers, which are sufficient to treat the faces of the truncated 3-D FDTD simulation region, the full 3-D ABC requires a three time-derivative Lorentz material in the edge and corner regions to achieve a rigorous matching of the resulting Maxwellian absorbing layers to the lossy medium. The 3-D ABC implementation thus requires the introduction of an auxiliary field to handle the edge and corner regions to achieve a state-space form of the update equations in the ABC layers. The desire to have a Maxwellian-based ABC extends beyond the numerical simplification it affords by avoiding the

Manuscript received August 24, 1998; revised October 5, 1999. The work by D. C. Wittwer was supported in part by the Radar Design Center, Raytheon Systems Company, Tucson, AZ, through the Doctoral Fellowship Program. The work by R. W. Ziolkowski was supported in part by the Office of Naval Research under Grant N0014-95-1-0636 and by the Air Force Office of Scientific Research, Air Force Material Command, USAF, under Grant F49620-96-1-0039. The views and conclusions contained herein are those of the author and should not be interpreted as necessarily representing the Office of Naval Research or the Air Force Office of Scientific Research or the U.S. Government.

The authors are with Electromagnetics Laboratory, Department of Electrical and Computer Engineering, University of Arizona, Tucson, AZ 85721-0104 USA.

Publisher Item Identifier S 0018-926X(00)01661-6.

field splitting associated with the PML ABC; it also allows for the possibility of potentially physically realizable materials for absorbers using the artificial material constructs discussed; for instance, in [25] and [26]. Complete details of the numerical implementation of the lossy 2TDLM (L2TDLM) ABC are presented. Comparisons between the L2TDLM ABC and the UPML ABC for the 2-D test cases presented in [4] and [8, ch. 5] are discussed. Fully 3-D examples including pulsed dipole radiation and pulsed Gaussian beam propagation in lossless and lossy materials as well as pulse propagation along a shielded microstrip line over lossless and lossy materials are included to illustrate the effectiveness of the L2TDLM ABC. We do not deal explicitly with evanescent wave issues associated with guided wave environments; rather we focus attention on the behavior of the L2TDLM ABC for source and propagation issues in both open and guided wave configurations. The applications of the L2TDLM ABC in a variety of MMIC configurations is presented elsewhere [27].

The derivation of the generalized formulation begins in Section II with an overview of the lossy two time-derivative Lorentz material (L2TDLM) model and its coupling to Maxwell's equations. Like the previous development in [1] we characterize a face (or slab) by its normal and introduce additional loss in that direction with an increasing profile function. To achieve a complete ABC we also introduce the requisite formulation for the edges (union of two faces, hence, depending on two independent loss profile parameters) and for the corners (union of three faces, hence, depending on three independent loss profile parameters). Like the previous development in [1], a formulation is introduced that reduces to the lossless case when the conductivity of the media becomes zero and which further reduces to Maxwell's equations in free-space as the permittivity goes to unity and, hence, recovers the 3-D TDLM ABC developed in [22]. It is highly desirable from a numerical implementation point of view to arrive at a formulation that has these properties. Furthermore, it is also highly convenient from an implementation point of view to have a formulation for a corner which reduces uniquely to the correct edge formulation and which further reduces uniquely to the correct face formulation with the appropriate selection of parameters. This avoids having separate formulations for each region, hence, makes the ABC very efficient to implement algorithmically and reduces the coding complexity. Differences between the previous formulation and the formulation presented here are identified and the selection of the parameter space is described. The discussion continues with the treatment of edges and corners. Finally, the formulation developed for the corner regions is demonstrated to reduce to the edge and face formulations as the appropriate parameters go to zero. The numerical implementation of the L2TDLM ABC is given in Section III and the numerical simulations used to quantify its performance are discussed in Section IV. Conclusions and future directions are presented in Section V.

II. L2TDLM ABC Derivation

Our foundation for engineering an absorbing material is based on the coupling of the electric and magnetic fields to polarization and magnetization currents. The coupling coefficients of the polarization and magnetization currents are then free parameters, which may be specified in such a way as to provide a reflectionless boundary between the surrounding homogeneous medium and the absorbing layer, which, following [15], is taken to be an uniaxial medium. Furthermore, the loss in the absorbing medium can be enhanced by varying the independent parameters of the polarization and magnetization currents as functions (profiles) of position away from an interface along the normal direction to that interface [1], [18]–[20], [22].

We wish to match a lossy dielectric medium to a uniaxial medium. The frequency-domain Maxwell's equations describing this uniaxial medium can be expressed in the following form:

$$\nabla \times \vec{\mathcal{E}} = -j\omega \left[\overline{\overline{\mu}} \right] \vec{\mathcal{H}}$$
$$\nabla \times \vec{\mathcal{H}} = j\omega \left[\overline{\overline{\epsilon}} \right] \vec{\mathcal{E}}$$

where we have defined as in [1] the tensors $\overline{\overline{\epsilon}}$ and $\overline{\overline{\mu}}$ for an interface with an x, y, z directed normal, respectively, by

$$\frac{\overline{\overline{\epsilon}}}{\epsilon_0} = \hat{\epsilon}_r \begin{pmatrix} 1/a_x & & \\ & a_x & \\ & & a_x \end{pmatrix} = \hat{\epsilon}_r \overline{\overline{\Lambda_x}}$$
$$\frac{\overline{\overline{\mu}}}{\mu_0} = \hat{\mu}_r \overline{\overline{\Lambda_x}}$$
$$\frac{\overline{\overline{\epsilon}}}{\epsilon_0} = \hat{\epsilon}_r \begin{pmatrix} a_y & & \\ & 1/a_y & \\ & & a_y \end{pmatrix} = \hat{\epsilon}_r \overline{\overline{\Lambda_y}}$$
$$\frac{\overline{\overline{\mu}}}{\mu_0} = \hat{\mu}_r \overline{\overline{\Lambda_y}}$$
$$\frac{\overline{\overline{\epsilon}}}{\epsilon_0} = \hat{\epsilon}_r \begin{pmatrix} a_z & & \\ & a_z & \\ & & 1/a_z \end{pmatrix} = \hat{\epsilon}_r \overline{\overline{\Lambda_z}}$$
$$\frac{\overline{\overline{\mu}}}{\mu_0} = \hat{\mu}_r \overline{\overline{\Lambda_z}}$$

where all of the off-diagonal terms are zero, the term $\hat{\epsilon}_r = \epsilon_r - j\sigma/\omega\epsilon_0$, the term $\hat{\mu}_r = \mu_r - j\sigma^*/\omega\mu_0$, and the terms a_x, a_y, and a_z correspond to the alteration of the material model in a direction transverse to the normal direction, which is labeled by the subscript. As was done in [1], these tensors are rewritten in terms of the electric and magnetic susceptibility tensors

$$\overline{\overline{\chi}}^e = \frac{\overline{\overline{\epsilon}}}{\epsilon_0} - \overline{\overline{1}}$$
$$\overline{\overline{\chi}}^m = \frac{\overline{\overline{\mu}}}{\mu_0} - \overline{\overline{1}}.$$

Consequently, the material parameters a_j are written below in terms of the material model susceptibilities as $a_j = 1 + \chi_{jj}$. We choose the absorber medium to be described by the two time-derivative Lorentz material model for lossy, dispersive media [1], denoted by L2TDLM, where time derivatives of the driving fields act as source terms to describe the coupling of the

electric and magnetic fields to the polarization and magnetization fields, [18]–[20], [22]. These polarization and magnetization field models are represented in differential form as

$$\frac{\partial^2}{\partial t^2}\mathcal{P}_x+\Gamma^e\frac{\partial}{\partial t}\mathcal{P}_x+\omega_o^2\mathcal{P}_x =\epsilon_0\left(\omega_p^2\chi_\alpha^e\mathcal{E}_x+\omega_p\chi_\beta^e\frac{\partial}{\partial t}\mathcal{E}_x+\chi_\gamma^e\frac{\partial^2}{\partial t^2}\mathcal{E}_x\right) \quad (1)$$

$$\frac{\partial^2}{\partial t^2}\mathcal{M}_x+\Gamma^m\frac{\partial}{\partial t}\mathcal{M}_x+\omega_o^2\mathcal{M}_x =\omega_p^2\chi_\alpha^m\mathcal{H}_x+\omega_p\chi_\beta^m\frac{\partial}{\partial t}\mathcal{H}_x+\chi_\gamma^m\frac{\partial^2}{\partial t^2}\mathcal{H}_x \quad (2)$$

where ω_0 is the resonance frequency and $\Gamma^{e,m}$ is the width of that resonance. The terms $\chi_\alpha^{e,m}$, $\chi_\beta^{e,m}$, and $\chi_\gamma^{e,m}$ represent, respectively, the coupling of the electric (magnetic) field and its first- and second-time derivatives to the local polarization (magnetization) fields. The term ω_p can be viewed as the plasma frequency associated with this coupling. It has been shown in [18] that if $\omega \gg \omega_0$, then the frequency-domain electric and magnetic susceptibilities associated, for instance, with (1) and (2) may be approximated in the frequency domain by

$$\chi_{xx}^e(\omega)=\frac{\mathcal{P}_x}{\epsilon_0\mathcal{E}_x}\approx-\frac{\omega_p^2}{\omega^2}\chi_\alpha^e-j\frac{\omega_p\chi_\beta^e}{\omega}+\chi_\gamma^e \quad (3)$$

$$\chi_{xx}^m(\omega)=\frac{\mathcal{M}_x}{\mathcal{H}_x}\approx-\frac{\omega_p^2}{\omega^2}\chi_\alpha^m-j\frac{\omega_p\chi_\beta^m}{\omega}+\chi_\gamma^m. \quad (4)$$

Following the arguments in [1], this material is readily matched to a lossy dielectric characterized by the material constants $\epsilon=\epsilon_r\epsilon_0$, $\mu=\mu_0$, and σ. One finds that matching is achieved when the free parameters in the L2TDLM model are given by

$$\omega_p^2\chi_\alpha^m=0 \quad (5)$$

$$\omega_p\chi_\beta^m=\rho_{\max}\rho(\vec{r}) \quad (6)$$

$$\chi_\gamma^m=0 \quad (7)$$

and

$$\omega_p^2\chi_\alpha^e=(\sigma/\epsilon_0)\omega_p\chi_\beta^m=(\sigma/\epsilon_0)\rho_{\max}\rho(\vec{r}) \quad (8)$$

$$\omega_p\chi_\beta^e=\sigma/\epsilon_0+\epsilon_r\omega_p\chi_\beta^m=(\sigma/\epsilon_0)+\epsilon_r\rho_{\max}\rho(\vec{r}) \quad (9)$$

$$\chi_\gamma^e=\epsilon_r-1. \quad (10)$$

We note that the term $\omega_p\chi_\beta^m$ is taken as a single quantity and is composed of a profile $0\le\rho(\vec{r})\le 1$ for increasing the loss while moving away from the interface along the normal direction and the profile maximum $\rho_{\max}$. For all the cases considered below, the profile was taken (as it was in [1]) to be a quadratic function of the distance away from the interface. These parameters represent the only independent values which must be specified to define the absorbing ABC layer. We also note that the form of the electric susceptibility reduces to the lossless case in the absence of the conductivity term. Furthermore, the electric susceptibility reduces to the free-space result as the permittivity approaches unity.

A. Faces

Consider a slab of absorber, which is matched to a lossy dielectric medium with the normal to its face being in the $+\hat{z}$ direction. Using our definition of $\overline{\overline{\epsilon}}$ and $\overline{\overline{\mu}}$ we define the electric and magnetic susceptibilities simply as

$$\overline{\overline{\chi}}^e=\hat{\epsilon}_r\overline{\overline{\Lambda_z}}-\overline{\overline{1}}$$
$$\overline{\overline{\chi}}^m=\overline{\overline{\Lambda_z}}-\overline{\overline{1}}.$$

The magnetization terms are identical to those treated in [22] and in [1]. On the other hand, the permittivity tensors must be handled as they were in [1], which is slightly different from their treatment in [22]. If we let $\zeta(z)$ represent the profile along z, the polarization field (1) combined with the L2TDLM material specifications (7)–(10) yield the following frequency domain expressions for the electric susceptibilities

$$\frac{P_{x,y}}{\epsilon_0E_{x,y}}=\chi_{xx,yy}^e(\omega)=\left[\hat{\epsilon}_r\overline{\overline{\Lambda_{x,y}}}-\overline{\overline{1}}\right]_{xx,yy}(\omega) =\frac{-\omega^2(\epsilon_r-1)+j\omega[\sigma/\epsilon_0+\epsilon_r\zeta]+\sigma\zeta/\epsilon_0}{-\omega^2}$$

$$\frac{P_z}{\epsilon_0E_z}=\chi_{zz}^e(\omega)=\left[\hat{\epsilon}_r\overline{\overline{\Lambda_z}}-\overline{\overline{1}}\right]_{zz}(\omega) =\frac{-\omega^2(\epsilon_r-1)+j\omega[\sigma/\epsilon_0-\zeta]}{-\omega^2+j\omega\zeta}.$$

The corresponding time-domain ordinary differential equations (ODE's) are

$$\partial_t^2\mathcal{P}_{x,y}=\epsilon_0(\epsilon_r-1)\partial_t^2\mathcal{E}_{x,y}+\epsilon_0[\sigma/\epsilon_0+\epsilon_r\zeta]\cdot\partial_t\mathcal{E}_{x,y}+\sigma\zeta\mathcal{E}_{x,y} \quad (11)$$

$$\partial_t^2\mathcal{P}_z+\zeta\partial_t\mathcal{P}_z=\epsilon_0(\epsilon_r-1)\partial_t^2\mathcal{E}_z+\epsilon_0[\sigma/\epsilon_0-\zeta]\partial_t\mathcal{E}_z. \quad (12)$$

To reduce these second-order ODE's to a first-order system that can be incorporated with Maxwell's equations, we introduce equations for the polarization currents $\partial_t\mathcal{P}_{x,y,z}$ in terms of the new variables $\mathcal{J}_{x,y,z}$ as

$$\partial_t\mathcal{P}_{x,y}=\mathcal{J}_{x,y}+\epsilon_0(\epsilon_r-1)\partial_t\mathcal{E}_{x,y}+[\sigma+\epsilon_r\epsilon_0\zeta]\mathcal{E}_{x,y} \quad (13)$$

$$\partial_t\mathcal{P}_z=\mathcal{J}_z+\epsilon_0(\epsilon_r-1)\partial_t\mathcal{E}_z+\sigma\mathcal{E}_z. \quad (14)$$

With these choices, the corresponding Maxwell's equations become

$$\partial_t\mathcal{E}_{x,y}=\frac{1}{\epsilon_0}\left(\nabla\times\vec{\mathcal{H}}\right)_{x,y}-\frac{1}{\epsilon_0}\partial_t\mathcal{P}_{x,y} =\frac{1}{\epsilon_0}\left(\nabla\times\vec{\mathcal{H}}\right)_{x,y}-\frac{1}{\epsilon_0}[\mathcal{J}_{x,y}+\epsilon_0(\epsilon_r-1)\partial_t\mathcal{E}_{x,y}+[\sigma+\epsilon_r\epsilon_0\zeta]\mathcal{E}_{x,y}]$$

$$\partial_t\mathcal{E}_z=\frac{1}{\epsilon_0}\left(\nabla\times\vec{\mathcal{H}}\right)_z-\frac{1}{\epsilon_0}\partial_t\mathcal{P}_z =\frac{1}{\epsilon_0}\left(\nabla\times\vec{\mathcal{H}}\right)_z-\frac{1}{\epsilon_0}\cdot[\mathcal{J}_z+\epsilon_0(\epsilon_r-1)\partial_t\mathcal{E}_z+\sigma\mathcal{E}_z].$$

These equations can be further reduced to the following forms which explicitly show the lossy nature of the ABC layer:

$$\partial_t \mathcal{E}_{x,y} + \left[\frac{\sigma}{\epsilon_r\epsilon_0} + \zeta\right]\mathcal{E}_{x,y} = \frac{1}{\epsilon_r\epsilon_0}\left(\nabla\times\vec{\mathcal{H}}\right)_{x,y} - \frac{1}{\epsilon_r\epsilon_0}\mathcal{J}_{x,y} \tag{15}$$

$$\partial_t \mathcal{E}_z + \frac{\sigma}{\epsilon_r\epsilon_0}\mathcal{E}_z = \frac{1}{\epsilon_r\epsilon_0}\left(\nabla\times\vec{\mathcal{H}}\right)_z - \frac{1}{\epsilon_r\epsilon_0}\mathcal{J}_z. \tag{16}$$

Using our choices for the polarization currents (13) and the Maxwell (15), we can arrive at the expression

$$\partial_t \mathcal{J}_{x,y} = \sigma\zeta\mathcal{E}_{x,y}. \tag{17}$$

The corresponding equation for the z component of the polarization field (12) combined with the polarization current definition (14) produces the relation

$$\partial_t \mathcal{J}_z + \zeta\mathcal{J}_z = -\zeta\epsilon_r\epsilon_0\partial_t\mathcal{E}_z - \sigma\zeta\mathcal{E}_z$$

that can be reduced with the corresponding Maxwell equation (16) to the following form

$$\begin{aligned}&\partial_t\mathcal{J}_z + \zeta\mathcal{J}_z\\ &= -\zeta\epsilon_r\epsilon_0\left[-\frac{\sigma}{\epsilon_r\epsilon_0}\mathcal{E}_z + \frac{1}{\epsilon_r\epsilon_0}\left(\nabla\times\vec{\mathcal{H}}\right)_z - \frac{1}{\epsilon_r\epsilon_0}\mathcal{J}_z\right] - \sigma\zeta\mathcal{E}_z\end{aligned}$$

and, hence, yields the desired expression for the z-component of the polarization current

$$\partial_t\mathcal{J}_z = -\zeta\left(\nabla\times\vec{\mathcal{H}}\right)_z. \tag{18a}$$

B. Edges

Consider the union of two slabs of absorber. Let, for example, one slab have its face normal to the $+\hat{x}$ direction and the other normal to the $+\hat{z}$ direction. To prevent reflections from an edge, the electric and magnetic susceptibilities must have the forms

$$\begin{aligned}\overline{\overline{\chi}}^e &= \hat{\epsilon}_r\overline{\overline{\Lambda_x}}\times\overline{\overline{\Lambda_z}} - \overline{\overline{1}}\\ \overline{\overline{\chi}}^m &= \overline{\overline{\Lambda_x}}\times\overline{\overline{\Lambda_z}} - \overline{\overline{1}}.\end{aligned}$$

Again, the magnetization terms are identical to those treated in [22] and the polarization terms must be handled separately. If we additionally let $\xi(x)$ represent the profile along x, the polarization fields are given by the frequency domain expressions as shown in (18b) at the bottom of the page. The corresponding time domain ODE's are

$$\begin{aligned}\partial_t^2\mathcal{P}_x + \xi\partial_t\mathcal{P}_x &= \epsilon_0(\epsilon_r-1)\partial_t^2\mathcal{E}_x + \epsilon_0[\sigma/\epsilon_0 + \epsilon_r\zeta - \xi]\\ &\quad\cdot\partial_t\mathcal{E}_x + \sigma\zeta\mathcal{E}_x \qquad (19)\\ \partial_t^3\mathcal{P}_y &= \epsilon_0(\epsilon_r-1)\partial_t^3\mathcal{E}_y + \epsilon_0[\sigma/\epsilon_0 + \epsilon_r(\xi+\zeta)]\\ &\quad\cdot\partial_t^2\mathcal{E}_y + \epsilon_0\left[\frac{\sigma}{\epsilon_0}(\xi+\zeta) + \epsilon_r\xi\zeta\right]\\ &\quad\partial_t\mathcal{E}_y + \sigma\xi\zeta\mathcal{E}_y \qquad (20)\\ \partial_t^2\mathcal{P}_z + \zeta\partial_t\mathcal{P}_z &= \epsilon_0(\epsilon_r-1)\partial_t^2\mathcal{E}_z + \epsilon_0[\sigma/\epsilon_0 + \epsilon_r\xi - \zeta]\\ &\quad\cdot\partial_t\mathcal{E}_z + \sigma\xi\mathcal{E}_z. \qquad (21)\end{aligned}$$

We note that second-order Lorentz models for the electric polarization fields arise in the components associated with the directions defining the edge while a third-order Lorentz model arises for the component normal to this edge. Again, to reduce these ODE's to a first-order system that can be incorporated with Maxwell's equations, we introduce equations for the polarization currents $\partial_t\mathcal{P}_{x,y,z}$ in terms of the new variables $\mathcal{J}_{x,y,z}$ as

$$\begin{aligned}\partial_t\mathcal{P}_x &= \mathcal{J}_x + \epsilon_0(\epsilon_r-1)\partial_t\mathcal{E}_x + (\sigma+\epsilon_r\epsilon_0\zeta)\mathcal{E}_x \qquad (22)\\ \partial_t\mathcal{P}_y &= \mathcal{J}_y + \epsilon_0(\epsilon_r-1)\partial_t\mathcal{E}_y + [\sigma+\epsilon_r\epsilon_0(\xi+\zeta)]\mathcal{E}_y \qquad (23)\\ \partial_t\mathcal{P}_z &= \mathcal{J}_z + \epsilon_0(\epsilon_r-1)\partial_t\mathcal{E}_z + (\sigma+\epsilon_r\epsilon_0\xi)\mathcal{E}_z \qquad (24)\end{aligned}$$

with these choices the corresponding Maxwell's equations become

$$\begin{aligned}\partial_t\mathcal{E}_x &= \frac{1}{\epsilon_0}\left(\nabla\times\vec{\mathcal{H}}\right)_x - \frac{1}{\epsilon_0}\partial_t\mathcal{P}_x\\ &= \frac{1}{\epsilon_0}\left(\nabla\times\vec{\mathcal{H}}\right)_x - \frac{1}{\epsilon_0}\\ &\quad\cdot[\mathcal{J}_x + \epsilon_0(\epsilon_r-1)\partial_t\mathcal{E}_x + (\sigma+\epsilon_r\epsilon_0\zeta)\mathcal{E}_x] \qquad (25)\\ \partial_t\mathcal{E}_y &= \frac{1}{\epsilon_0}\left(\nabla\times\vec{\mathcal{H}}\right)_y - \frac{1}{\epsilon_0}\partial_t\mathcal{P}_y\\ &= \frac{1}{\epsilon_0}\left(\nabla\times\vec{\mathcal{H}}\right)_y - \frac{1}{\epsilon_0}\\ &\quad\cdot[\mathcal{J}_y + \epsilon_0(\epsilon_r-1)\partial_t\mathcal{E}_y + [\sigma+\epsilon_r\epsilon_0(\xi+\zeta)]\mathcal{E}_y] \qquad (26)\\ \partial_t\mathcal{E}_z &= \frac{1}{\epsilon_0}\left(\nabla\times\vec{\mathcal{H}}\right)_z - \frac{1}{\epsilon_0}\partial_t\mathcal{P}_z\\ &= \frac{1}{\epsilon_0}\left(\nabla\times\vec{\mathcal{H}}\right)_z - \frac{1}{\epsilon_0}\\ &\quad\cdot[\mathcal{J}_z + \epsilon_0(\epsilon_r-1)\partial_t\mathcal{E}_z + (\sigma+\epsilon_r\epsilon_0\xi)\mathcal{E}_z]. \qquad (27)\end{aligned}$$

$$\begin{aligned}\frac{P_x}{\epsilon_0E_x} &= \frac{-\omega^2(\epsilon_r-1) + j\omega[\sigma/\epsilon_0 + \epsilon_r\zeta - \xi] + \sigma\zeta/\epsilon_0}{-\omega^2 + j\omega\xi}\\ \frac{P_y}{\epsilon_0E_y} &= \frac{(j\omega)(-\omega^2)(\epsilon_r-1) - \omega^2[\sigma/\epsilon_0 + \epsilon_r(\xi+\zeta)] + j\omega\left[\frac{\sigma}{\epsilon_0}(\xi+\zeta) + \epsilon_r\xi\zeta\right] + \sigma\xi\zeta/\epsilon_0}{(j\omega)(-\omega^2)}\\ \frac{P_z}{\epsilon_0E_z} &= \frac{-\omega^2(\epsilon_r-1) + j\omega[\sigma/\epsilon_0 + \epsilon_r\xi - \zeta] + \sigma\xi/\epsilon_0}{-\omega^2 + j\omega\zeta}\end{aligned} \tag{18b}$$

These equations can be simplified to the following set, which clearly shows the lossy nature of the medium:

$$\partial_t \mathcal{E}_x + \left(\frac{\sigma}{\epsilon_r\epsilon_0} + \zeta\right)\mathcal{E}_x = \frac{1}{\epsilon_r\epsilon_0}\left(\nabla\times\vec{\mathcal{H}}\right)_x - \frac{1}{\epsilon_r\epsilon_0}\mathcal{J}_x \tag{28}$$

$$\partial_t \mathcal{E}_y + \left[\frac{\sigma}{\epsilon_r\epsilon_0} + (\xi+\zeta)\right]\mathcal{E}_y = \frac{1}{\epsilon_r\epsilon_0}\left(\nabla\times\vec{\mathcal{H}}\right)_y - \frac{1}{\epsilon_r\epsilon_0}\mathcal{J}_y \tag{29}$$

$$\partial_t \mathcal{E}_z + \left(\frac{\sigma}{\epsilon_r\epsilon_0} + \xi\right)\mathcal{E}_z = \frac{1}{\epsilon_r\epsilon_0}\left(\nabla\times\vec{\mathcal{H}}\right)_z - \frac{1}{\epsilon_r\epsilon_0}\mathcal{J}_z. \tag{30}$$

Again, using our choices for the polarization currents (22)–(24), we can arrive at

$$\begin{aligned}
\partial_t^2\mathcal{P}_x + \xi\partial_t\mathcal{P}_x &= \partial_t\mathcal{J}_x + \epsilon_0(\epsilon_r-1)\partial_t^2\mathcal{E}_x \\
&\quad + (\sigma+\epsilon_r\epsilon_0\zeta)\partial_t\mathcal{E}_x + \xi\mathcal{J}_x \\
&\quad + \xi\epsilon_0(\epsilon_r-1)\partial_t\mathcal{E}_x + \xi(\sigma+\epsilon_r\epsilon_0\zeta)\mathcal{E}_x \\
&= \epsilon_0(\epsilon_r-1)\partial_t^2\mathcal{E}_x \\
&\quad + (\sigma+\epsilon_r\epsilon_0\zeta-\epsilon_0\xi)\partial_t\mathcal{E}_x + \sigma\zeta\mathcal{E}_x \\
\partial_t\mathcal{J}_x + \xi\mathcal{J}_x &= -\xi\epsilon_r\epsilon_0\partial_t\mathcal{E}_x \\
&\quad + [\sigma(\zeta-\xi) - \epsilon_r\epsilon_0\xi]\mathcal{E}_x \\
&= -\xi\epsilon_r\epsilon_0\left[-\left(\frac{\sigma}{\epsilon_r\epsilon_0}+\zeta\right)\mathcal{E}_x\right. \\
&\quad \left. + \frac{1}{\epsilon_r\epsilon_0}\left(\nabla\times\vec{\mathcal{H}}\right)_x - \frac{1}{\epsilon_r\epsilon_0}\mathcal{J}_x\right] \\
&\quad + [\sigma(\zeta-\xi) - \epsilon_r\epsilon_0\xi]\mathcal{E}_x.
\end{aligned}$$

The first relation yields the equation for the x component of the electric current

$$\partial_t\mathcal{J}_x = -\xi\left(\nabla\times\vec{\mathcal{H}}\right)_x + \sigma\zeta\mathcal{E}_x. \tag{31}$$

The corresponding equation for the z component of the current can be found by symmetry to be

$$\partial_t\mathcal{J}_z = -\zeta\left(\nabla\times\vec{\mathcal{H}}\right)_z + \sigma\xi\mathcal{E}_z. \tag{32}$$

The remaining equation for the y component of the electric current is determined from the third-order Lorentz model for the electric polarization field (20) as follows:

$$\begin{aligned}
\partial_t^3\mathcal{P}_y &= \partial_t^2\mathcal{J}_y + \epsilon_0(\epsilon_r-1)\partial_t^3\mathcal{E}_y \\
&\quad + [\epsilon_r\epsilon_0(\xi+\zeta)+\sigma]\partial_t^2\mathcal{E}_y \\
&= \epsilon_0(\epsilon_r-1)\partial_t^3\mathcal{E}_y + [\epsilon_r\epsilon_0(\xi+\zeta)+\sigma]\partial_t^2\mathcal{E}_y \\
&\quad + \epsilon_0\left[\frac{\sigma}{\epsilon_0}(\xi+\zeta) + \epsilon_r\xi\zeta\right]\partial_t\mathcal{E}_y + \sigma\xi\zeta\mathcal{E}_y.
\end{aligned}$$

This leads immediately to a second-order ODE for $\mathcal{J}_y$

$$\partial_t^2\mathcal{J}_y = [\sigma(\xi+\zeta) + \epsilon_r\epsilon_0\xi\zeta]\partial_t\mathcal{E}_y + \sigma\xi\zeta\mathcal{E}_y.$$

This second-order ODE for $\mathcal{J}_y$ is dealt with by introducing the auxiliary function $\mathcal{F}_y$ as defined by

$$\partial_t\mathcal{J}_y = \mathcal{F}_y + [\sigma(\xi+\zeta) + \epsilon_r\epsilon_0\xi\zeta]\mathcal{E}_y. \tag{33}$$

This represents the desired rate equation for the y component of the electric current. It then follows that the auxiliary function must satisfy the corresponding rate equation

$$\partial_t\mathcal{F}_y = \sigma\xi\zeta\mathcal{E}_y. \tag{34a}$$

We note that this auxiliary function is identically zero when the conductivity goes to zero.

C. Corners

Finally, consider the union of three slabs of absorber, one slab having its face normal to the $+\hat{x}$, one normal to the $+\hat{y}$, and one normal to the $+\hat{z}$ direction. To prevent reflections from a corner, the electric and magnetic susceptibilities must have the forms:

$$\begin{aligned}
\overline{\overline{\chi}}^{\,e} &= \hat{\epsilon}_r\,\overline{\overline{\Lambda_x}}\times\overline{\overline{\Lambda_y}}\times\overline{\overline{\Lambda_z}} - \overline{\overline{1}} \\
\overline{\overline{\chi}}^{\,m} &= \overline{\overline{\Lambda_x}}\times\overline{\overline{\Lambda_x}}\times\overline{\overline{\Lambda_z}} - \overline{\overline{1}}.
\end{aligned}$$

Again, the magnetization terms are identical to those treated in [22] and the polarization terms must be handled separately. With the form of the susceptibility matrix, one finds each term is related to all the others simply by a cyclic permutation of the indices. Thus, if we additionally let $\eta(y)$ represent the profile along y, the polarization field, for instance, along the z axis is given by the frequency domain expression as shown in (34b) at the bottom of the page.

The resulting time domain ODE is then found to be

$$\begin{aligned}
\partial_t^3\mathcal{P}_z + \zeta\partial_t^2\mathcal{P}_z &= \epsilon_0(\epsilon_r-1)\partial_t^3\mathcal{E}_z \\
&\quad + \epsilon_0[\sigma/\epsilon_0 + \epsilon_r(\xi+\eta-\zeta)]\partial_t^2\mathcal{E}_z \\
&\quad + \epsilon_0\left[\frac{\sigma}{\epsilon_0}(\xi+\eta) + \epsilon_r\xi\eta\right]\partial_t\mathcal{E}_z + \sigma\xi\eta\mathcal{E}_z.
\end{aligned}$$

We note that a third-order Lorentz model for the electric polarization field again arises in 3-D for the corners. We make the following choice for the polarization current:

$$\partial_t\mathcal{P}_z = \mathcal{J}_z + \epsilon_0(\epsilon_r-1)\partial_t\mathcal{E}_z + [\sigma + \epsilon_r\epsilon_0(\xi+\eta)]\mathcal{E}_z. \tag{35}$$

$$\frac{P_z}{\epsilon_0 E_z} = \frac{(j\omega)(-\omega^2)(\epsilon_r-1) - \omega^2[\sigma/\epsilon_0 + \epsilon_r(\xi+\eta-\zeta)] + j\omega[\sigma(\xi+\eta)/\epsilon_0 + \epsilon_r\xi\eta] + \sigma\xi\eta/\epsilon_0}{(j\omega)(-\omega^2) - \zeta\omega^2} \tag{34b}$$

We then find Maxwell's equation for the z component of the electric field to be

$$\begin{aligned}\partial_t \mathcal{E}_z &= \frac{1}{\epsilon_0}\left(\nabla\times\vec{\mathcal{H}}\right)_z - \frac{1}{\epsilon_0}\partial_t \mathcal{P}_z \\ &= \frac{1}{\epsilon_0}\left(\nabla\times\vec{\mathcal{H}}\right)_z - \frac{1}{\epsilon_0} \\ &\quad\cdot\left[\mathcal{J}_z + \epsilon_0(\epsilon_r-1)\partial_t\mathcal{E}_z + [\sigma+\epsilon_r\epsilon_0(\xi+\eta)]\mathcal{E}_z\right]\end{aligned}$$

which reduces to the lossy medium relation

$$\partial_t \mathcal{E}_z + \left[\frac{\sigma}{\epsilon_r\epsilon_0} + (\xi+\eta)\right]\mathcal{E}_z = \frac{1}{\epsilon_r\epsilon_0}\left(\nabla\times\vec{\mathcal{H}}\right)_z - \frac{1}{\epsilon_r\epsilon_0}\mathcal{J}_z. \tag{36}$$

Using the choice (35) for the polarization current, one obtains

$$\begin{aligned}&\partial_t^3\mathcal{P}_z + \zeta\partial_t^2\mathcal{P}_z \\ &\quad= \partial_t^2\mathcal{J}_z + \epsilon_0(\epsilon_r-1)\partial_t^3\mathcal{E}_z \\ &\qquad+ [\sigma+\epsilon_r\epsilon_0(\xi+\eta)]\,\partial_t^2\mathcal{E}_z + \zeta\partial_t\mathcal{J}_z \\ &\qquad+ \zeta\epsilon_0(\epsilon_r-1)\partial_t^2\mathcal{E}_z + \zeta\left[\sigma+\epsilon_r\epsilon_0(\xi+\eta)\right]\partial_t\mathcal{E}_z \\ &\quad= \epsilon_0(\epsilon_r-1)\partial_t^3\mathcal{E}_z + \epsilon_0\left[\sigma/\epsilon_0 + \epsilon_r(\xi+\eta-\zeta)\right]\partial_t^2\mathcal{E}_z \\ &\qquad+ \epsilon_0\left[\frac{\sigma}{\epsilon_0}(\xi+\eta) + \epsilon_r\xi\eta\right]\partial_t\mathcal{E}_z + \sigma\xi\eta\mathcal{E}_z\end{aligned}$$

which yields a current equation of the form

$$\begin{aligned}\partial_t^2\mathcal{J}_z + \zeta\partial_t\mathcal{J}_z = &-\zeta\epsilon_r\epsilon_0\partial_t^2\mathcal{E}_z \\ &+ [\epsilon_r\epsilon_0(\xi\eta - \zeta(\xi+\eta)) \\ &\quad+\sigma(\xi+\eta-\zeta)]\,\partial_t\mathcal{E}_z + \sigma\xi\eta\mathcal{E}_z.\end{aligned}$$

Again, we introduce the auxiliary function $\mathcal{F}_z$ defined by the following ODE

$$\begin{aligned}\partial_t\mathcal{J}_z + \zeta\mathcal{J}_z = &\mathcal{F}_z - \zeta\epsilon_r\epsilon_0\partial_t\mathcal{E}_z \\ &+ [\epsilon_r\epsilon_r(\xi\eta - \zeta(\xi+\eta)) + \sigma(\xi+\eta-\zeta)]\,\mathcal{E}_z.\end{aligned} \tag{37}$$

The second-order equation for $\mathcal{J}_z$ can then be reduced to the relation

$$\begin{aligned}\partial_t\mathcal{J}_z + \zeta\mathcal{J}_z &= \mathcal{F}_z - \zeta\epsilon_r\epsilon_0\partial_t\mathcal{E}_z \\ &\quad+ [\epsilon_r\epsilon_r(\xi\eta - \zeta(\xi+\eta)) + \sigma(\xi+\eta-\zeta)]\,\mathcal{E}_z \\ &= \mathcal{F}_z - \zeta\epsilon_r\epsilon_0\left[-\left[\frac{\sigma}{\epsilon_r\epsilon_0} + (\xi+\eta)\right]\mathcal{E}_z\right. \\ &\qquad\left.+\frac{1}{\epsilon_r\epsilon_0}\left(\nabla\times\vec{\mathcal{H}}\right)_z - \frac{1}{\epsilon_r\epsilon_0}\mathcal{J}_z\right] \\ &\quad+ [\epsilon_r\epsilon_r(\xi\eta - \zeta(\xi+\eta)) + \sigma(\xi+\eta-\zeta)]\,\mathcal{E}_z.\end{aligned}$$

The following first-order ODE's for $\mathcal{F}_z$ and $\mathcal{J}_z$ are then obtained:

$$\partial_t\mathcal{J}_z = -\zeta\left(\nabla\times\vec{\mathcal{H}}\right)_z + [\epsilon_r\epsilon_0\xi\eta + \sigma(\xi+\eta)]\,\mathcal{E}_z + \mathcal{F}_z \tag{38}$$

$$\partial_t\mathcal{F}_z = \sigma\xi\eta\mathcal{E}_z. \tag{39}$$

We note that if in the corner equations we set $\eta = 0$ (or $\xi = 0$ or $\zeta = 0$), which would be appropriate for the corner reducing to an x–z edge (or y–z edge or x–y edge, respectively), the equations obtained in the previous subsection for that edge are recovered. Similarly, the corner equations with two profile parameters set to zero or the edge equations with one profile parameter set to zero recover the corresponding face equations. This self-consistency of the equations significantly reduces the complexity of coding the L2TDLM ABC. Moreover, it also significantly reduces the operation counts required to implement the L2TDLM ABC from those associated with Berenger's PML ABC, particularly in the face and edge regions, which account for the majority of the layers associated with these ABC's.

III. Implementation

These polarization, magnetization and auxiliary field rate equations are implemented into a FDTD simulator by obtaining their discrete forms using finite differences. Consider, for instance, the z component set of equations for the corner

$$\begin{aligned}\partial_t\mathcal{E}_z + \left[\frac{\sigma}{\epsilon_r\epsilon_0} + (\xi+\eta)\right]\mathcal{E}_z &= \frac{1}{\epsilon_r\epsilon_0}\left(\nabla\times\vec{\mathcal{H}}\right)_z - \frac{1}{\epsilon_r\epsilon_0}\mathcal{J}_z \\ \partial_t\mathcal{J}_z = -\zeta\left(\nabla\times\vec{\mathcal{H}}\right)_z &+ [\epsilon_r\epsilon_0\xi\eta + \sigma(\xi+\eta)]\,\mathcal{E}_z + \mathcal{F}_z \\ \partial_t\mathcal{F}_z &= \sigma\xi\eta\mathcal{E}_z.\end{aligned}$$

For convenience, we define the quantities

$$A = \frac{\sigma}{\epsilon_r\epsilon_0} + (\xi+\eta) \tag{40}$$

$$B = -\zeta \tag{41}$$

$$C = \epsilon_r\epsilon_0\xi\eta + \sigma(\xi+\eta) \tag{42}$$

$$D = \sigma\xi\eta \tag{43}$$

to simplify the form of the equation system as

$$\partial_t\mathcal{E}_z + A\mathcal{E}_z = \frac{1}{\epsilon_r\epsilon_0}\left(\nabla\times\vec{\mathcal{H}}\right)_z - \frac{1}{\epsilon_r\epsilon_0}\mathcal{J}_z \tag{44}$$

$$\partial_t\mathcal{J}_z = +B\left(\nabla\times\vec{\mathcal{H}}\right)_z + C\mathcal{E}_z + \mathcal{F}_z \tag{45}$$

$$\partial_t\mathcal{F}_z = D\mathcal{E}_z. \tag{46}$$

If we let these fields be located at $\mathcal{E}_z^{n,n+1}$, $\mathcal{J}_z^{n,n+1}$, and $\mathcal{F}_z^{n+1/2}$ and introduce an exponential difference scheme, the simplified system then takes the discrete form

$$\begin{aligned}\mathcal{E}_z^{n+1} &= \exp(-A\Delta t)\mathcal{E}_z^n + \frac{\Delta t}{\epsilon_r\epsilon_0}\exp(-A\Delta t/2) \\ &\quad\cdot\left[\left(\nabla\times\vec{\mathcal{H}}\right)_z^{n+1/2} - \left(\frac{\mathcal{J}_z^{n+1}+\mathcal{J}_z^n}{2}\right)\right] \\ \mathcal{J}_z^{n+1} &= \mathcal{J}_z^n + \Delta t B\left(\nabla\times\vec{\mathcal{H}}\right)_z^{n+1/2} \\ &\quad+ \Delta t C\left(\frac{\mathcal{E}_z^{n+1}+\mathcal{E}_z^n}{2}\right) + \Delta t\mathcal{F}_z^{n+1/2} \\ \mathcal{F}_z^{n+1/2} &= \mathcal{F}_z^{n-1/2} + \Delta t D\mathcal{E}_z^n.\end{aligned}$$

These update equations for $\mathcal{E}_z$ and $\mathcal{J}_z$ can be rewritten in a state-space matrix form

$$\overline{\overline{A}}\begin{pmatrix}\mathcal{E}_z\\ \mathcal{J}_z\end{pmatrix}^{n+1} = \overline{\overline{B}}\begin{pmatrix}\mathcal{E}_z\\ \mathcal{J}_z\end{pmatrix}^{n} + \overline{\overline{C}}\begin{pmatrix}\left(\nabla\times\vec{\mathcal{H}}\right)_z\\ \mathcal{F}_z\end{pmatrix}^{n+1/2}$$

where the matrices

$$\begin{aligned}\overline{\overline{A}} &= \begin{bmatrix} a_{11} & a_{12} \\ a_{21} & a_{22} \end{bmatrix} \\ &= \begin{bmatrix} 1 & (\Delta t/2\epsilon_r\epsilon_0)\exp(-A\Delta t/2) \\ -\Delta t C/2 & 1 \end{bmatrix} \end{aligned} \tag{47}$$

$$\begin{aligned}\overline{\overline{B}} &= \begin{bmatrix} b_{11} & b_{12} \\ b_{21} & b_{22} \end{bmatrix} \\ &= \begin{bmatrix} \exp(-A\Delta t) & -(\Delta t/2\epsilon_r\epsilon_0)\exp(-A\Delta t/2) \\ \Delta t C/2 & 1 \end{bmatrix} \end{aligned} \tag{48}$$

$$\begin{aligned}\overline{\overline{C}} &= \begin{bmatrix} c_{11} & c_{12} \\ c_{21} & c_{22} \end{bmatrix} \\ &= \begin{bmatrix} (\Delta t/\epsilon_r\epsilon_0)\exp(-A\Delta t/2) & 0 \\ \Delta t B & \Delta t \end{bmatrix}. \end{aligned} \tag{49}$$

This state–space system has the explicit solution

$$\begin{aligned}&\begin{pmatrix} \mathcal{E}_z \\ \mathcal{J}_z \end{pmatrix}^{n+1} \\ &= \frac{1}{\det\left(\overline{\overline{A}}\right)} \begin{bmatrix} a_{22}b_{11} - a_{12}b_{21} & a_{22}b_{12} - a_{12}b_{22} \\ a_{11}b_{21} - a_{21}b_{11} & a_{11}b_{22} - a_{21}b_{12} \end{bmatrix} \begin{pmatrix} \mathcal{E}_z \\ \mathcal{J}_z \end{pmatrix}^{n} \\ &\quad + \frac{1}{\det\left(\overline{\overline{A}}\right)} \begin{bmatrix} a_{22}c_{11} - a_{12}c_{21} & a_{22}c_{12} - a_{12}c_{22} \\ a_{11}c_{21} - a_{21}c_{11} & a_{11}c_{22} - a_{21}c_{12} \end{bmatrix} \\ &\quad \cdot \begin{pmatrix} \left(\nabla \times \vec{\mathcal{H}}\right)_z \\ \mathcal{F}_z \end{pmatrix}^{n+1/2}. \end{aligned}$$

We then finally arrive at the semi-implicit update equations

$$\begin{aligned}\mathcal{E}_z^{n+1} &= \frac{a_{22}b_{11} - a_{12}b_{21}}{\det\left(\overline{\overline{A}}\right)} \mathcal{E}_z^n + \frac{a_{22}c_{11} - a_{12}c_{21}}{\det\left(\overline{\overline{A}}\right)} \\ &\quad \cdot \left(\nabla \times \vec{\mathcal{H}}\right)_z^{n+1/2} + \frac{a_{22}b_{12} - a_{12}b_{22}}{\det\left(\overline{\overline{A}}\right)} \mathcal{J}_z^n \\ &\quad + \frac{a_{22}c_{12} - a_{12}c_{22}}{\det\left(\overline{\overline{A}}\right)} \mathcal{F}_z^{n+1/2} \end{aligned} \tag{50}$$

$$\begin{aligned}\mathcal{J}_z^{n+1} &= \frac{a_{11}b_{22} - a_{21}b_{12}}{\det\left(\overline{\overline{A}}\right)} \mathcal{J}_z^n + \frac{a_{11}c_{21} - a_{21}c_{11}}{\det\left(\overline{\overline{A}}\right)} \\ &\quad \cdot \left(\nabla \times \vec{\mathcal{H}}\right)_z^{n+1/2} + \frac{a_{11}b_{21} - a_{21}b_{11}}{\det\left(\overline{\overline{A}}\right)} \mathcal{E}_z^n \\ &\quad + \frac{a_{11}c_{22} - a_{21}c_{12}}{\det\left(\overline{\overline{A}}\right)} \mathcal{F}_z^{n+1/2} \end{aligned} \tag{51}$$

$$\mathcal{F}_z^{n+3/2} = \mathcal{F}_z^{n+1/2} + \Delta t D \mathcal{E}_z^{n+1}. \tag{52}$$

Similar equations occur for the x and y components. They can be obtained immediately from this set by cyclic permutations of the indices and profile parameters. These L2TDLM ABC update equations reduce to the corresponding TDLM ABC update equations given in [22] when $\sigma \to 0$ and $\epsilon_r \to 1$. Note that one of the main reasons that the exponential differencing scheme was selected here was to ensure this reduction. Similar numerical results can be obtained for the L2TDLM ABC using a more direct central differencing scheme.

IV. Numercial Results

The L2TDLM ABC developed above has been implemented in a 3-D FDTD simulator, and the quality of absorption provided by it has been evaluated. Several 3-D problems have been used to test the efficacy of the L2TDLM ABC including: 1) a Hertzian dipole radiator in a homogeneous lossy medium; 2) a Gaussian beam incident from free space onto a homogeneous lossy medium; and 3) a shielded microstrip transmission line with a lossy homogeneous dielectric substrate. In all these validation examples, a numerical reflection coefficient due to the introduction of the L2TDLM ABC is calculated by first running simulations with a large spatial extent to define the reference solution. Simulations with a smaller simulation space, which was truncated with the L2TDLM ABC, were then performed. Electric field quantities were monitored at fixed locations in both cases and compared. Their Fourier spectra were then obtained via a discrete Fourier transform. The difference between the calculated truncated and reference field spectra normalized by the calculated reference field spectrum was used to generate the numerical reflection coefficient. This spectral domain information thus allowed us to quantify the numerical reflection coefficient introduced by the L2TDLM ABC as a function of the frequency.

The following descriptions of the test problems indicate the internal dimensions of the simulation. Additional cells that are required by the L2TDLM ABC are to be added onto the total sizes cited below. Unless otherwise noted, the L2TDLM ABC layers were taken to be ten cells thick.

A. Comparisons with Gedney's UPML ABC

Comparisons between the L2TDLM ABC and the TDLM ABC for the 2-D cases discussed in [20] and between the UPML ABC for the 2-D cases discussed in [4] and [8, Ch. 5] were run to provide initial test results. A 2-D version of the 3-D L2TDLM ABC is straightforwardly obtained from (50)–(52). The update equations are essentially those for the faces and edges, but no auxiliary field variable needs to be introduced into the update system. The out-of-plane component of the electric field is not excited in this reduced dimensionality problem. A code was constructed to test the 2-D L2TDLM ABC. The cases in [20] provided basic algorithmic checks since, as noted above, the L2TDLM ABC reduces to the TDLM ABC when the losses go to zero and the medium becomes free-space. All of the results obtained in [20] were reproduced with the L2TDLM ABC algorithm.

Next, Gedney's test case [4] and [8, ch. 5] was considered. It is a two medium problem in which the simulation space is split into two homogeneous half-spaces: one air, the other a lossy medium with $\epsilon_r = 10.0$ and $\sigma = 0.3$ S/m. The normal to the

interface is selected to be the $\hat{y}$-direction. The source is a electric dipole strip $J_y(x_c, z_c, t)$ driven with the Gaussian derivative time signal

$$J_y(x_c, z_c, t) = -2\left[\frac{t-t_0}{t_w}\right]\exp\left[-\left(\frac{t-t_0}{t_w}\right)^2\right] \tag{53}$$

where $t_w = 26.53$ ps and $t_0 = 4t_w$. The spectrum of this driving pulse has its peak at an effective frequency of $f_{\text{eff}} = 8.45$ GHz where $\Delta \sim \lambda/35.5$, but extends out to 40 GHz where $\Delta \sim \lambda/7.5$. The strip is oriented along the normal to the interface and is located in the free-space region at two cells above the center of the simulation space. The simulation space consisted of 40×40 square cells and was truncated with a ten-layer quadratic L2TDLM ABC. The reference simulation region was 1240×1240 square cells and was terminated with perfect electric conductors. The cell size was $\Delta = 0.4$ mm. We introduce a grid frequency, $f_{\text{grid}} = c/(40.0\Delta_{\max})$, where $\Delta_{\max}$ is the maximum of the cell side lengths Δx, Δy, or Δz; it corresponds to the lowest frequency at which the grid provides a $\lambda/40$ discretization level. Thus, for the cubical grid associated with this problem, $f_{\text{grid}} = 1.875 \times 10^{10}$ Hz. The simulation was run for 1000 time steps, the time step being set at 0.98 of the Courant value. Standard differentiation, while maintaining the semi-implicit formulation, rather than exponential differencing was used to make the 2-D L2TDLM ABC algorithm as close as possible to Gedney's UPML. The problem is treated in a 2-D TE polarization sense; the field components (E_x, E_y, and H_z) are obtained with the FDTD simulator. The maximum relative errors $\mathcal{E}_A$ and $\mathcal{E}_B$ in E_y are measured, respectively, at the point A, which is located in free-space two cells above the interface and two cells from one face of the ABC region, and at the point B, which is located two cells from each face of one of the corners in the lossy medium. The maximum relative error in E_y is defined as the difference in time between the amplitude of E_y for the small problem and for the reference problem normalized by the maximum in time of E_y for the reference result. Note that like Gedney's UPML ABC, only a single maximum parameter is used throughout the L2TDLM ABC. This simplifies the coding requirements significantly. The maximum parameter that gave the best error results in the split region problem corresponded to the best value for the free-space case.

Using the L2TDLM ABC it was found that $\mathcal{E}_A = -76.4$ dB and $\mathcal{E}_B = -73.0$ dB with a maximum loss parameter $\rho_{\max}/\omega_{\text{grid}} = 7.13$. Changing the profile of the ABC layers to a quartic variation yielded the errors $\mathcal{E}_A = -85.9$ dB and $\mathcal{E}_B = -71.8$ dB with a maximum loss parameter $\rho_{\max}/\omega_{\text{grid}} = 12.3$. These results are comparable to those reported by Gedney. This problem is a quite difficult one in which to assess the difference in errors between points A and B because the time signals arriving at these two points are dramatically different. The pulse reaching point B is nearly a derivative of the excitation pulse, hence, the peak of its frequency spectrum is upshifted significantly. Moreover, because of the field pattern from the source, different sides of the ABC are illuminated differently. We felt, like Gedney, that these levels of reflection errors are quite satisfactory considering the fact that the discretization is below $\lambda_{\text{medium}}/10$ for a significant portion of the frequency spectrum of the signals reaching the sampling points.

However, to connect these 2-D results with those in [5], [6], and [20], the corresponding line source problem was also treated. Instead of the electric strip, the problem is now excited by a magnetic line source K_z driven with the time signal used in the cases in [20]:

$$K_z(x_c, z_c, t) = \begin{cases} \dfrac{1}{320}[10 - 15\cos(\omega_0 t) \\ \quad +6\cos(2\omega_0 t) - \cos(3\omega_0 t)] & \text{for } 0 \le t \le 1.0 \text{ ns} \\ 0, & \text{for } t > 1.0 \text{ ns} \end{cases} \tag{54}$$

where $\omega_0 = 2.0\pi \times 10^9$. The advantage of this source is that the faces and corners of the simulation region see essentially the same time signal. The cell size was $\Delta = 0.6$ mm; hence, $f_{\text{grid}} = 1.25 \times 10^{10}$ Hz.

In our first series of 2-D simulations, the simulation region was free space. We obtained $\mathcal{E}_A = -96.2$ dB and $\mathcal{E}_B = -74.7$ dB for a maximum loss parameter $\rho_{\max}/\omega_{\text{grid}} = 10.20$ and $\mathcal{E}_A = -84.9$ dB and $\mathcal{E}_B = -81.4$ dB for a maximum loss parameter $\rho_{\max}/\omega_{\text{grid}} = 9.17$. The latter case provided the best overall error performance for a variety of sampling points. These results indicate that the edge and corner errors vary with the choice of the maximum parameter. The more uniform maximum relative error seems to be the most beneficial choice for standard application problems. In our second series of 2-D simulations, the simulation region was completely filled with the lossy dielectric having $\epsilon_r = 10.0$ and $\sigma = 0.3$ S/m. It was found that $\mathcal{E}_A = -92.5$ dB and $\mathcal{E}_B = -91.7$ dB with a maximum loss parameter $\rho_{\max}/\omega_{\text{grid}} = 3.06$, approximately $\sqrt{10}$ smaller than its free-space value. In our third series of 2-D simulations, the simulation region, as it was in Gedney's test case, was half-filled with free space and with the same lossy medium. The line source K_z was now excited in free-space, two cells away from the center of the simulation region along the normal to the interface. It was found that $\mathcal{E}_A = -93.8$ dB and $\mathcal{E}_B = -81.0$ dB with a maximum loss parameter $\rho_{\max}/\omega_{\text{grid}} = 9.17$. All of these results demonstrate excellent reflectionless behavior.

Finally, we ran our 3-D L2TDLM ABC simulator for the corresponding 3-D problem of a vertical electric dipole located in free space 2 cells above the same lossy half-space. The simulation space consisted of $40 \times 40 \times 40$ cubic cells and was truncated with a ten-layer quadratic L2TDLM ABC. The reference simulation region was $140 \times 140 \times 140$ cubic cells and was terminated with the same ten-layer quadratic L2TDLM ABC. The cell size was again $\Delta = 0.4$ mm; hence, $f_{\text{grid}} = 1.875 \times 10^{10}$ Hz. The simulation was run for 1000 time steps, the time step being set at the Courant value. The electric dipole was driven with the time signal (53). We obtained $\mathcal{E}_A = -74.7$ dB and $\mathcal{E}_B = -78.6$ dB for a maximum loss parameter $\rho_{\max}/\omega_{\text{grid}} = 9.0$. These results are comparable with those obtained in the 2-D simulations. We note that while the 2-D L2TDLM ABC exhibited a much slower late time growth of the error over the indicated simulation time than Gedney's 2-D UPML ABC, the 3-D

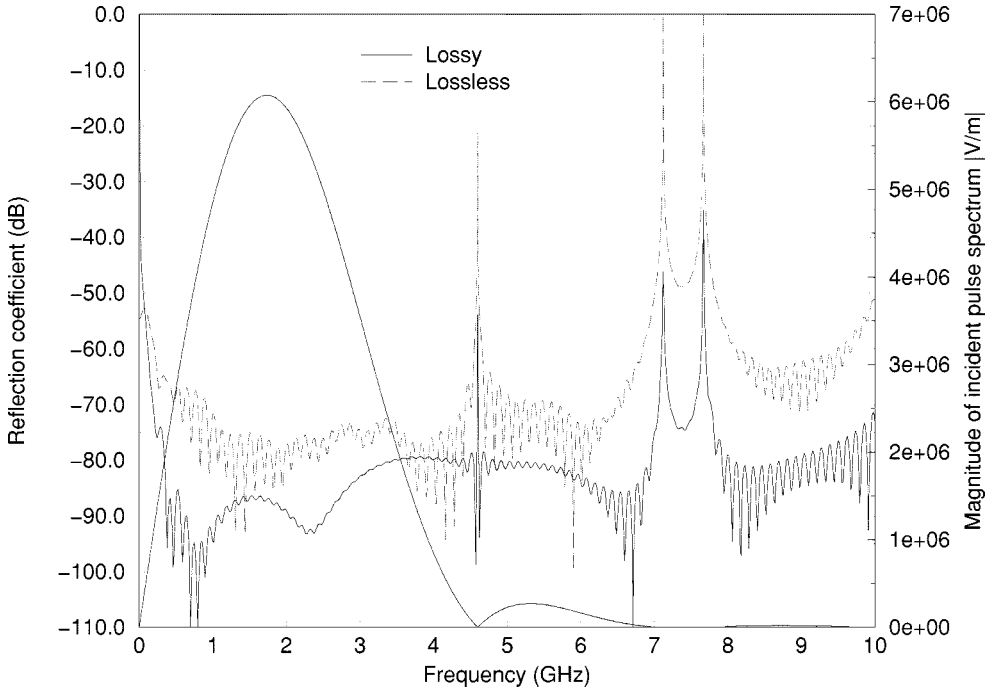

Fig. 1. Incident pulse spectrum and reflection coefficients for the pulsed Hertzian dipole radiator case. The peak frequency of the incident pulse was 1.7 GHz. The discretizations were $\Delta x = \Delta y = \Delta z = \lambda_{\text{eff}}/40$, where $f_{\text{eff}} = 3.1$ GHz.

L2TDLM ABC simulation showed no growth over the same simulation time. Similar to the free-space TDLM results [22], the largest error occurred for the leading wave front and settled into a much lower average value.

B. Hertzian Dipole Radiator

The Hertzian dipole radiator in a homogeneous region is one of the most fundamental radiation problems. It made an excellent candidate for our initial validation purposes in 3-D. Additionally, since comparisons between the TDLM and PML ABC's were provided for the free space version of this 3-D problem in [22], we could check our L2TDLM ABC algorithm against those results in that limit.

The reference (140 × 140 × 140 cells) and trial (40 × 40 × 40 cells) solutions were excited with a bipolar pulse having an effective (root mean square) frequency of $f_{\text{eff}} = 3.1$ GHz (the peak of the spectrum of the driving pulse is at 1.7 GHz). The discretization was set at $\lambda_{\text{eff}}/40$; hence $f_{\text{grid}} = f_{\text{eff}}$. This is equivalent to a cell size of $\Delta x = \Delta y = \Delta z = 2.42$ mm. The corresponding time step was taken at the CFL = 1.0 limit and, hence, $\Delta t = 4.656$ ps. The simulation was run for 2000 time steps. The L2TDLM ABC was placed on all six faces. The current element was placed at $[(71, 71, 70)_{\text{ref}}, (21, 21, 20)_{\text{trial}}]$ to locate it exactly in the middle of the simulation region. The $\hat{z}$ electric field was sampled 15 cells (36.3 mm) away at the points $[(71, 56, 71)_{\text{ref}}, (21, 6, 21)_{\text{trial}}]$.

The simulation region was first filled with a lossless dielectric, ($\epsilon_r = 2.0$, $\sigma = 0.0$), and the numerical reflection coefficient due to the L2TDLM ABC was calculated. The ξ, η, and ζ profile functions were all taken to be the same. The associated parameter $\rho_{\max}$ was obtained with several simulation runs to optimize the performance of the L2TDLM ABC; its value was chosen to be $\rho_{\max}/\omega_{\text{grid}} = 8.0$. This value was held fixed for each of the dipole source examples. The simulation was then run again using a lossy dielectric, ($\epsilon_r = 2.0$, $\sigma = 0.167$). This is a highly lossy dielectric having an equivalent loss tangent, $\tan\delta = 0.1$, at 3.0 GHz.

Fig. 1 displays the results of these computations. The spectrum of the excitation pulse is provided to define the relevant frequencies. The L2TDLM ABC provides a reflection coefficient smaller than −75 dB for the lossless case and smaller than −85 dB for the lossy case over the frequency band of interest (≈0–4.5 GHz). It is important to note that the discretization (cells/λ_{diel}) at the highest usable frequency (4.5 GHz) is ≈15 cells/λ_{diel}. In other words, the incident pulse spectrum is fairly well resolved over the entire bandwidth. It also indicates why the error increases further with increasing frequency. Thus, the L2TDLM ABC is very effective for truncati es and lossy materials. Note that the spikes in the reflection coefficients occur where the excitation spectrum has a null; hence, they are due to the normalization. While the incident field has no energy at those frequencies, numerical dispersion results in noise contributions there. Thus the noise in the grid at those frequencies divided by essentially noise resulting from the discrete Fourier transform there produces large reflection coefficients. This signature is present in all of the results presented below.

C. Pulsed Gaussian Beam Incident on a Homogeneous Slab

The pulsed Gaussian beam problem is of particular interest because it allows us to investigate the behavior of the L2TDLM ABC as the incident energy propagates across a dielectric interface. Moreover, unlike the dipole case, it allows us to test the effectiveness of the L2TDLM ABC in a finite beam scattering problem. Furthermore, unlike the shielded microstrip case to

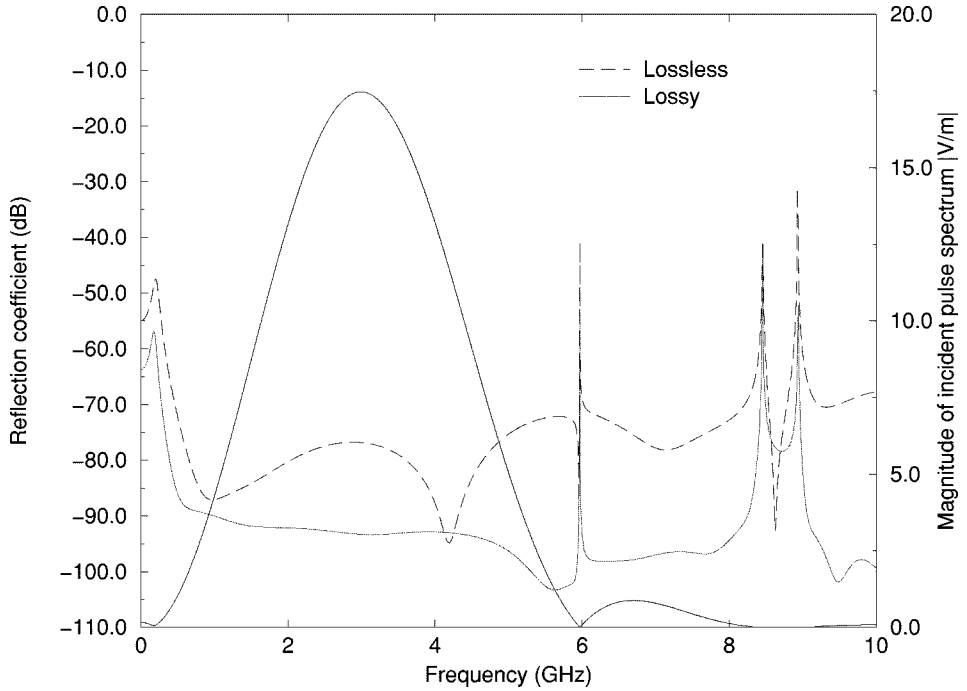

Fig. 2. Incident pulse spectrum and reflection coefficients for a pulsed Gaussian beam incident on a lossy dielectric half-space ($\epsilon_r = 1.0,\ \sigma = 0.0,\ 0.167$). The peak frequency of the incident pulse was 3.0 GHz. The discretizations were $\Delta x = \Delta y = \Delta z = \lambda_{\rm peak}/20$.

follow, the field energy is propagating normal to the interface as opposed to parallel to the interface as it does in the shielded microstrip problem.

The reference ($100 \times 100 \times 100$ cells) and trial ($100 \times 100 \times 60$ cells) solutions where discretized at $\lambda_{\rm eff}/20$, $\lambda_{\rm eff}$ being the wavelength associated with the effective frequency, and $f_{\rm eff} = 3.0$ GHz (the peak of the spectrum of the driving pulse). This is equivalent to a cell size of $\Delta x = \Delta y = \Delta z = 5.0$ mm; hence, $f_{\rm grid} = f_{\rm eff}/2$. The corresponding time step was taken at the CFL = 1.0 limit and, hence, $\Delta t = 9.623$ ps. The simulation was run for 250 time steps. The L2TDLM ABC was again placed on all six faces of the simulation region. The ξ, η, and ζ ABC profile functions again were all taken to be the same. The ABC parameter $\rho_{\max}$ was obtained with several simulation runs to optimize the performance of the L2TDLM ABC. The Gaussian beam was polarized in the $\hat{x}$ direction and propagated in the $\hat{z}$ direction. The beam was excited on a total/scattered field boundary located in the $z = 10\Delta z$ plane. A dielectric half-space was introduced in the $z = 20\Delta z$ plane. This dielectric half-space extends into the L2TDLM ABC regions. The x component of the electric field was sampled 28 cells (140.0 mm) away from the L2TDLM interface at the point (50, 50, 38).

The dielectric half-space was first filled with vacuum ($\epsilon_r = 1.0,\ \sigma = 0.0$) and the numerical reflection coefficient calculated. Although not of practical interest, the effect of adding conductivity without the presence of a relative dielectric constant was examined. The half-space was filled with a lossy medium, ($\epsilon_r = 1.0,\ \sigma = 0.167$), which has an equivalent loss tangent $\tan\,\delta = 0.1$ at 3.0 GHz. The ABC parameter $\rho_{\max}$ was chosen to be $\rho_{\max}/\omega_{\rm grid} = 5.0$ for both cases. Fig. 2 shows both numerical reflection coefficients introduced by truncating the simulation region with the L2TDLM ABC. Again, it also includes the spectrum of the pulse excitation.

Excellent absorption is provided by the absorbing layer with relatively coarse discretization. The L2TDLM ABC produces reflections less than -75 dB over the bandwidth of the pulse for the free-space case. Introduction of the conductivity in the half-space region further reduces the reflection introduced by the boundary to less than -90 dB. This is in part due to propagation loss but proves that the L2TDLM ABC is stable and effective in simulations utilizing lossy media.

The properties of the L2TDLM ABC were further investigated with dielectric materials. Initially, the reflection coefficient introduced by the ABC was calculated with a lossless dielectric ($\epsilon_r = 2.0,\ \sigma = 0.0$) filling the half-space. This calculation was repeated using a lossy dielectric ($\epsilon_r = 2.0,\ \sigma = 0.167$). Again, the ABC parameter $\rho_{\max}$ was chosen to be $\rho_{\max}/\omega_{\rm grid} = 5.0$ for both cases. Fig. 3 shows both numerical reflection coefficients introduced by the L2TDLM ABC. The spectrum of the incident field is provided again to focus attention on the relevant frequencies.

The lossless case shows better than -75 dB reflection over the frequency bandwidth of the pulse. The monotonically increasing characteristic of the reflection coefficient caused suspicion of under sampling at the higher frequencies. It was found that the effective discretization in the dielectric was $\lambda_{\rm diel}/14$ at 3.0 GHz where $\lambda_{\rm diel} = \lambda_{\rm eff}/\sqrt{2}$, which meant that the effective discretization in the dielectric was approximately $\lambda_{\rm diel}/20$ at 2.0 GHz and only $\lambda_{\rm diel}/10$ at 4.0 GHz. This is not sufficient sampling for the entire frequency bandwidth of the driving pulse; especially when proper modeling of any dispersive behavior is desired. Regardless, the lossy dielectric case produced a reflection less than -110 dB over the frequency bandwidth of the incident pulse.

The effect of under sampling at the higher frequencies in the incident pulse was investigated by increasing the discretization

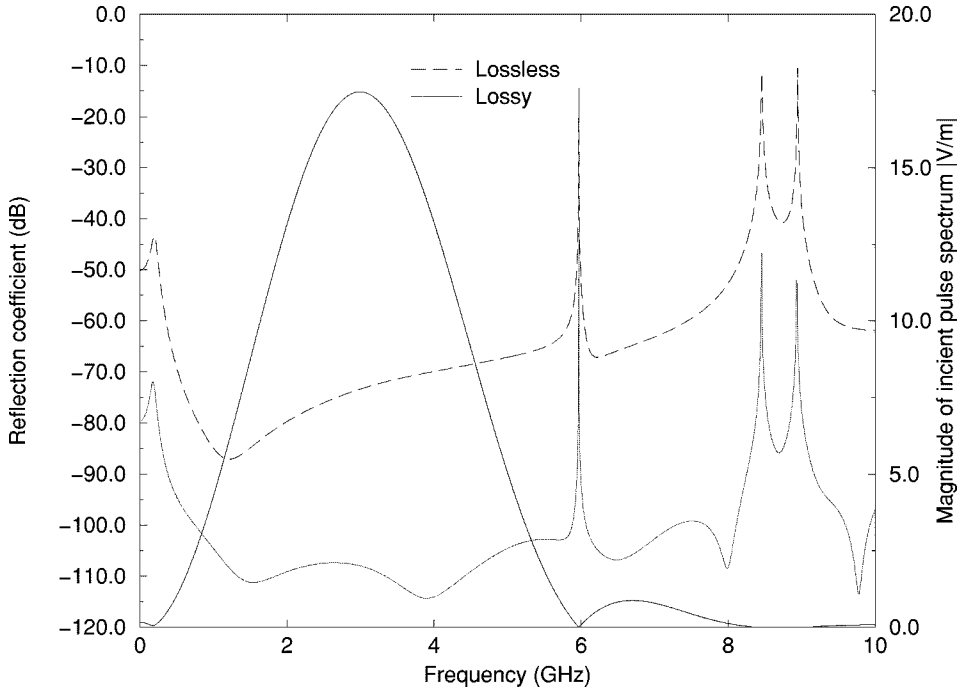

Fig. 3. Incident pulse spectrum and reflection coefficients for a pulsed Gaussian beam incident on a lossy dielectric half-space ($\epsilon_r = 2.0,\ \sigma = 0.0,\ 0.167$). The peak frequency of the incident pulse was 3.0 GHz. The discretizations were $\Delta x = \Delta y = \Delta z = \lambda_{\rm peak}/20$.

by 50%. The reference and trial solutions were scaled appropriately to (150 × 150 × 150) and (150 × 150 × 120) cells, respectively. At an effective frequency of $f_{\rm eff} = 3.0$ GHz and a discretization of $\lambda_{\rm eff}/30$, the cell size is $\Delta x = \Delta y = \Delta z = 3.33$ mm and $f_{\rm grid} = 0.75 f_{\rm eff}$. The simulation was run at the CFL = 1.0 limit, hence, with $\Delta t = 6.415$ ps, for 600 time steps for a total time of 3.85 ns. Again the L2TDLM ABC was placed on all six faces of the simulation domain. The same source was used. The total/scattered field boundary is located in the $z = 20\,\Delta z$ plane. The air/dielectric interface is located in the $z = 30\,\Delta z$ plane. The x component of the electric field was sampled at (75, 75, 57) which is 123.2 mm in front of the total/scattered field boundary and 89.9 mm in front of the air/dielectric interface. The ABC parameter $\rho_{\max}$ was chosen to be $\rho_{\max}/\omega_{\rm grid} = 5.5$ for the lossless case and $\rho_{\max}/\omega_{\rm grid} = 5.0$ for the lossy case. Both the lossless and lossy dielectric cases were run again. The resulting numerical reflection obtained at this discretization is shown in Fig. 4.

The lossless reflection coefficient is less than −75 dB over the frequency bandwidth of the pulse. The increase in discretization removed the monotonically increasing behavior of the reflection coefficient. The increased resolution improved the lossy case to better than −115 dB over the frequency bandwidth of the pulse. Smaller discretizations were not performed since the memory requirements would have exceeded the available memory on our machines. These pulsed Gaussian beam results were in good agreement with those calculated previously with those presented in [1].

D. Shielded Microstrip

Finally, we also considered the very practical printed circuit problem of modeling a shielded microstrip propagating into a L2TDLM ABC. This problem is encountered in many EMI/EMC problems. It is quite different from the previous problems in that it is a guided wave problem that allows unipolar pulse excitations, i.e., pulses with nonzero spectra at dc.

The reference (24 × 50 × 500 cells) and trial (24 × 50 × 50 cells) solutions where discretized at $\lambda_{\rm eff}/283.5$ in the $\hat{x}$ and $\hat{y}$ directions and $\lambda_{\rm eff}/100$ in the $\hat{z}$ direction. The effective frequency was $f_{\rm eff} = 25.0$ GHz. The equivalent cell sizes are $\Delta x = \Delta y = 0.043$ mm and $\Delta z = 0.120$ mm; hence, $f_{\rm grid} = 2.5 f_{\rm eff}$. The corresponding time step at the CFL = 1.0 limit and, hence, $\Delta t = 96.80$ fs. The simulation was run for 2000 time steps. The 2TDLM ABC was placed only on the $\hat{z}$ normal faces with the other faces being perfect electric conductors (PEC). The dielectric substrate ($\epsilon_r = 2.2$) was six cells (0.72 mm) thick in the $\hat{x}$ direction. The microstrip was modeled as infinitely thin, being six cells (0.72 mm) wide and starting in the $z = 10\,\Delta z$ plane. The microstrip line was excited by a $\hat{x}$ directed current source having a Gaussian time history with spectral width as shown in Fig. 5 and an effective cutoff frequency of approximately 30 GHz. The x component of the electric field was sampled 16 cells (3.24 mm) away from the source plane at the point (3, 26, 37). The interface between the air and dielectric region was treated by using an average of the neighboring permittivity values for the field quantities which lie on the interface.

The simulation region was first filled with a lossless dielectric ($\epsilon_r = 2.2,\ \sigma = 0.0$). With several simulation runs to optimize the performance of the L2TDLM ABC, the parameter $\rho_{\max}$ was chosen to have a value $\rho_{\max}/\omega_{\rm grid} = 50.0$ for the lossless case. The numerical reflection coefficient due to the L2TDLM ABC was then calculated. The simulation was then run again using a lossy dielectric ($\epsilon_r = 2.2,\ \sigma = 0.167$). This is a highly lossy dielectric having an equivalent loss tangent

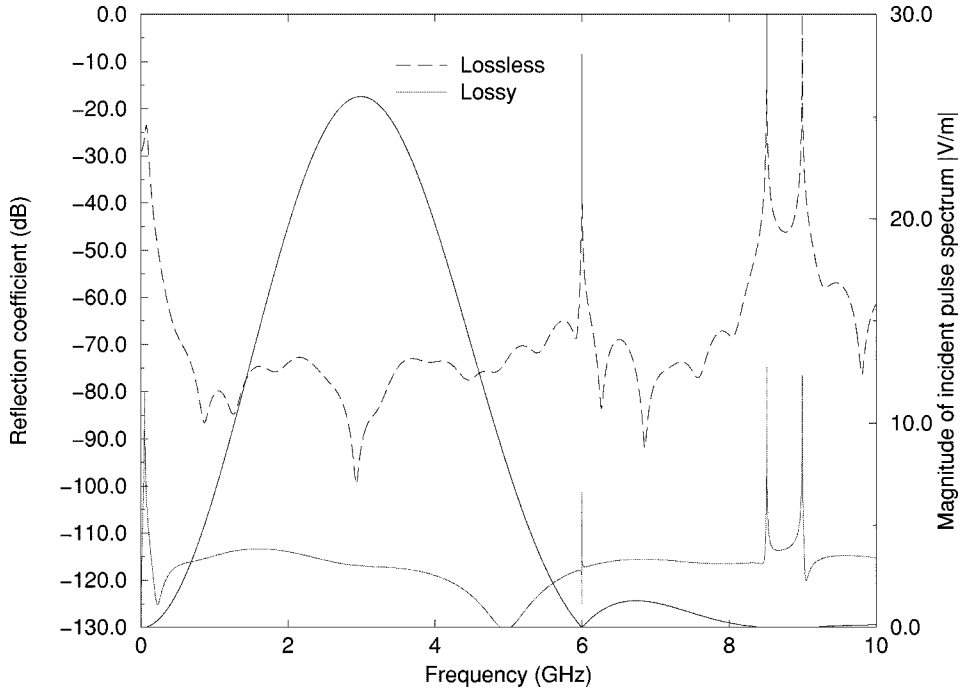

Fig. 4. Incident pulse spectrum and reflection coefficients for a pulsed Gaussian beam incident on a lossy dielectric half-space ($\epsilon_r = 2.0,\ \sigma = 0.0,\ 0.167$). The peak frequency of the incident pulse was 3.0 GHz. The discretizations were $\Delta x = \Delta y = \Delta z = \lambda_{\text{peak}}/30$.

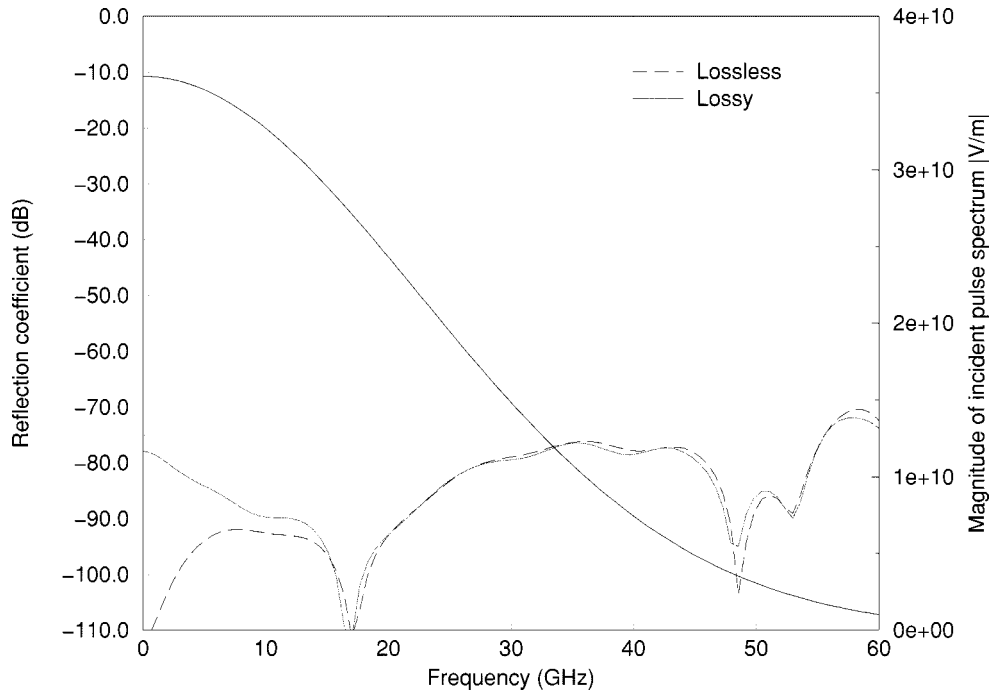

Fig. 5. Incident pulse spectrum and reflection coefficients for a shielded microstrip transmission line over a lossy substrate ($\epsilon_r = 2.2,\ \sigma = 0.0,\ 0.167$). The effective frequency of the incident Gaussian pulse was 25.0 GHz.

$\tan\delta = 0.015$, at 25.0 GHz. Similar optimization runs led to the value $\rho_{\max}/\omega_{\text{grid}} = 30.0$ for the lossy case. The numerical reflection coefficient due to the L2TDLM ABC was then calculated for the lossy substrate case.

Fig. 5 displays the results of these computations. It demonstrates that the L2TDLM ABC provides for a reflection coefficient better than -75 dB for both the lossless and lossy cases over the frequency band of interest ($\approx$0–30.0 GHz). At the upper edge of the frequency band (30.0 GHz), the discretization is ≈ 83 cells/λ_{eff} in the air region and ≈ 56 cells/λ_{diel} within the dielectric region for the $\hat{z}$ direction and is a much finer resolution than that in the transverse directions. The incident pulse spectrum is significantly over sampled for the entire bandwidth. Again, the interface between the air and dielectric region was treated as an average of the neighboring permittivity values for field quantities which lie on the interface.

TABLE I
SUMMARY OF NUMERICAL REFLECTION COEFFICIENT RESULTS

Numerical reflection coefficient

Test Problem	ϵ_r	σ [S/m^2]	Reflection Coefficient [dB]
Hertzian electric dipole			
	2.0	0.000	$\leq$ 75
	2.0	0.167	$\leq$ 85
Gaussian beam ($\lambda_{diel}/20$)			
	1.0	0.000	$\leq$ 75
	1.0	0.167	$\leq$ 90
	2.0	0.000	$\leq$ 70
	2.0	0.167	$\leq$ 110
($\lambda_{diel}/30$)			
	2.0	0.000	$\leq$ 75
	2.0	0.167	$\leq$ 115
Shielded Microstrip			
	2.2	0.000	$\leq$ 75
	2.2	0.167	$\leq$ 75

The physical size of the absorber is an important issue for discussion, especially when one would like to simulate structures with detail much smaller than the wavelength in the medium. It was found previously [16] that the effectiveness of the Berenger PML ABC [9] was reliant on the physical size of absorber to be a significant fraction of the wavelength in the medium. This does not appear to be the case in this instance. The absorber is only 1/8 of a wavelength in free space and 1/5 of a wavelength in the dielectric. It is felt that this is the case because most of the energy is normally incident on the L2TDLM ABC in this guided wave situation.

V. CONCLUSIONS AND FUTHER WORK

A generalized lossy two time-derivative Lorentz material (L2TDLM) model absorbing boundary condition (ABC) has been introduced. The advantage of the generalized formulation presented here is that only one equation set is required in the implementation for all parts of the ABC region. This equation set reduces to the appropriate formulation (corner to edge to face) dependent on the number of independent parameters present in a given portion of the simulation region. A complete 3-D FDTD implementation was described and its performance was evaluated using several two and three dimensional test cases. The results of these 3-D test cases is summarized in the Table I. They demonstrate that the L2TDLM ABC is a very effective technique for truncating FDTD simulation regions dealing with lossy media.

Several practical applications involving the L2TDLM ABC including micropatch antennas, microstrip filters and couplers have also been investigated. The results of these studies are summarized in [27].

REFERENCES

[1] D. C. Wittwer and R. W. Ziolkowski, "Two time-derivative Lorentz material (2TDLM) formulation of a Maxwellian absorbing layer matched to a lossy medium," *IEEE Trans. Antennas Propagat.*, vol. 48, pp. 192–199, Feb. 2000.

[2] S. Gedney, "An anisotropic perfectly matched layer—Absorbing medium for the truncation of FDTD lattices," *IEEE Trans. Antennas Propagat.*, vol. 44, pp. 1630–1639, Dec. 1996.

[3] C. M. Rappaport and S. C. Winton, "Modeling dispersive soil for FDTD computation by fitting conductivity parameters," in *Proc. Appl. Computat. Electromagn. Soc.*, Monterey, CA, Mar. 1997, pp. 112–117.

[4] S. D. Gedney, "An anisotropic PML absorbing media for FDTD simulation of fields in lossy dispersive media," *Electromagn.*, vol. 16, pp. 399–415, July/Aug. 1996.

[5] Y. C. Lau, M. S. Leong, and P. S. Kooi, "Extension of Berenger's PML boundary condition in matching lossy medium and evanescent waves," *Electron. Lett.*, vol. 32, no. 11, pp. 974–976, 1996.

[6] J. Fang and Z. Wu, "Generalized perfect matched layer for the absorption of propagating and evanescent waves in lossless and lossy media," *IEEE Trans. Microwave Theory Tech.*, vol. 14, pp. 2216–2222, Dec. 1996.

[7] Q. H. Liu, "An FDTD algorithm with perfectly matched layers for conductive media," *Microwave Opt. Technol. Lett.*, vol. 14, pp. 134–137, Feb. 1997.

[8] A. Taflove, *Advances in Computational Electrodynamics: The Finite-Difference Time-Domain Method*. Boston, MA: Artech House, 1998.

[9] J.-P. Berenger, "A perfectly matched layer for the absorption of electromagnetic waves," *J. Comp. Phys.*, vol. 114, pp. 185–200, Oct. 1994.

[10] D. S. Katz, E. T. Thiele, and A. Taflove, "Validation and extension to three dimensions of the Berenger PML absorbing boundary condition for FD-TD meshes," *IEEE Microwave Guided Wave Lett.*, vol. 4, pp. 268–270, Aug. 1994.

[11] W. C. Chew and W. H. Weedon, "A 3-D perfectly matched medium from modified Maxwell's equations with stretched coordinates," *Microwave Opt. Technol. Lett.*, vol. 7, no. 9, pp. 599–604, Sept. 1994.

[12] C. E. Reuter, R. M. Joseph, E. T. Thiele, D. S. Katz, and A. Taflove, "Ultrawideband absorbing boundary condition for termination of waveguiding structures in FDTD simulations," *IEEE Microwave Guided Wave Lett.*, vol. 4, pp. 246–344, Oct. 1994.

[13] C. M. Rappaport, "Perfectly matched absorbing boundary conditions based on anisotropic lossy mapping of space," *IEEE Microwave Guided Wave Lett.*, vol. 5, pp. 90–92, Mar. 1995.

[14] R. Mittra and Ü. Pekel, "A new look at the perfectly matched layer (PML) concept for the reflectionless absorption of electromagnetic waves," *IEEE Microwave Guided Wave Lett.*, vol. 5, pp. 84–86, Mar. 1995.

[15] Z. S. Sacks, D. M. Kingsland, R. Lee, and J.-F. Lee, "A perfectly matched anisotropic absorber for use as an absorbing boundary condition," *IEEE Trans. Antennas Propagat.*, vol. 43, pp. 1460–1463, Dec. 1995.

[16] D. C. Wittwer and R. W. Ziolkowski, "How to design the imperfect Berenger PML," *Electromagn.*, vol. 16, pp. 465–485, July/Aug. 1996.

[17] L. Zhao and A. C. Cangellaris, "GT-PML: Generalized theory of perfectly matched layers and its application to the reflectionless truncation of finite-difference time-domain grids," *IEEE Trans. Microwave Theory Tech.*, vol. 44, pp. 2555–2563, Dec. 1996.

[18] R. W. Ziolkowski, "The design of Maxwellian absorbers for numerical boundary conditions and for practical applications using engineered artificial materials," *IEEE Trans. Antennas Propagat.*, vol. 45, pp. 656–671, Apr. 1997.

[19] ——, "Time-derivative Lorentz materials and their utilization as electromagnetic absorbers," *Phys. Rev. E*, vol. 55, no. 6, pp. 7696–7703, June 1997.

[20] ——, "Time-derivative Lorentz material model-based absorbing boundary condition," *IEEE Trans. Antennas Propagat.*, vol. 45, pp. 1530–1535, Oct. 1997.

[21] P. G. Petropoulos, A. C. Cangellaris, and L. Zhao, "A reflectionless sponge layer absorbing boundary condition for the solution of Maxwell's equations with high-order staggered finite difference schemes," *J. Computat. Phys.*, vol. 139, no. 1, pp. 184–208, Jan. 1998.

[22] R. W. Ziolkowski, "Maxwellian material based absorbing boundary conditions," *Comput. Methods. Appl. Mech. Engrg.*, vol. 169, pp. 237–262, 1999.

[23] E. Turkel and A. Yefet, "Absorbing PML boundary layers for wave-like equations,", preprint, July 1997, to be published.

[24] S. Abarbanel and D. Gottlieb, "On the construction and analysis of absorbing layers in CEM," in *Proc. Appl. Computat. Electromagn. Soc.*, Monterey, CA, Mar. 1997, pp. 876–883.

[25] F. Auzanneau and R. W. Ziolkowski, "Theoretical study of synthetic bianisotropic materials," *J. Electromagn. Waves Applicat.*, vol. 12, no. 3, pp. 353–370, Dec. 1997.

[26] ——, "Microwave signal rectification using artificial composite materials composed of diode loaded, electrically small dipole antennas," *IEEE Trans. Microwave Theory Tech.*, vol. 46, pp. 1628–1637, Nov. 1998.

[27] D. C. Wittwer and R. W. Ziolkowski, "The effect of dielectric loss in FDTD simulations of microstrip structures," IEEE Trans. Microwave Theory Tech., Oct. 1998, submitted for publication.

David C. Wittwer (S'93–M'95) received the B.S., M.S., and Ph.D. degrees in electrical engineering from the Department of Electrical and Computer Engineering at the University of Arizona, Tucson, AZ, in 1993, 1995, and 1998, respectively.

He was a Member of the technical staff at Hughes Missile Systems Company in Tucson, AZ, from 1995 to 1999. While at Hughes, he received the Howard Hughes Doctoral Fellowship. His work at Hughes involved the analysis, design and measurement of microstrip and slot arrays for missile seeker and telemetry antennas. In 1999 he joined the assembly and test development group at Intel Corporation in Chandler, AZ, where he is a Senior Packaging Engineer. His focus area is in electromagnetic compatibility and interference compliance of computer microprocessors. His research interests include the development and implementation of time-domain electromagnetic solvers.

Dr. Wittwer is a member of the IEEE Antennas and Propagation, Microwave Theory and Techniques, and Electromagnetic Compatibility societies.

Richard W. Ziolkowski (M'87–SM'91–F'94) received the Sc.B. degree in physics *magna cum laude* (with honors) from Brown University, Providence, RI, in 1974, and the M.S. and Ph.D. degrees in physics from the University of Illinois at Urbana-Champaign, in 1975 and 1980, respectively.

From 1981 to 1990, he was a member of the Engineering Research Division at the Lawrence Livermore National Laboratory and served as the Leader of the Computational Electronics and Electromagnetics Thrust Area for the Engineering Directorate from 1984 to 1990. He joined the Department of Electrical and Computer Engineering at the University of Arizona as an Associate Professor in 1990 and was promoted to Full Professor in 1996. He was a coguest editor of the 1998 feature issue of the *Journal of the Optical Society of America A* on mathematics and modeling in modern optics. His research interests include the application of new mathematical and numerical methods to linear and nonlinear problems dealing with the interaction of acoustic and electromagnetic waves with realistic materials and structures.

Dr. Ziolkowski is a member of Tau Beta Pi, Sigma Xi, and Phi Kappa Phi, the American Physical Society, the Optical Society of America, the Acoustical Society of America, and Commissions B (Fields and Waves) and D (Electronics and Photonics) of URSI (International Union of Radio Science). He was an Associate Editor for the IEEE TRANSACTIONS ON ANTENNAS AND PROPAGATION from 1993 to 1998. He served as the Vice Chairman of the 1989 IEEE/AP-S and URSI Symposium in San Jose, CA, and as the Technical Program Chairperson for the 1998 IEEE Conference on Electromagnetic Field Computation in Tucson, AZ. For the U.S. URSI Commission B, he served as Secretary from 1993 to 1996 and as Chairperson of the Technical Activities Committee from 1997 to 1999. He will serve as a Member-at-Large of the U.S. National Committee (USNC) of URSI in 2000. He was a coorganizer of the Photonics Nanostructures Special Symposia at the 1998 and 1999 OSA Integrated Photonics Research Topical Meetings. He was awarded the Tau Beta Pi Professor of the Year Award in 1993 and the IEEE and Eta Kappa Nu Outstanding Teaching Award in 1993 and 1998, respectively.